POLITECNICO DI TORINO
Repository ISTITUZIONALE

Cluster charge-density-wave glass in hydrogen-intercalated TiSe2

Original
Cluster charge-density-wave glass in hydrogen-intercalated TiSe2 / Prando, G., Piatti, E., Daghero, D., Gonnelli, R.S., Carretta, P.. - In: PHYSICAL REVIEW MATERIALS. - ISSN 2475-9953. - 7:9(2023). [10.1103/PhysRevMaterials.7.094002]

Availability:
This version is available at: 11583/2981854 since: 2023-09-09T14:23:47Z

Publisher:
American Physical Society

Published
DOI:10.1103/PhysRevMaterials.7.094002

Terms of use:

This article is made available under terms and conditions as specified in the corresponding bibliographic description in the repository

Publisher copyright
APS postprint/Author's Accepted Manuscript e postprint versione editoriale/Version of Record

This article appeared in PHYSICAL REVIEW MATERIALS, 2023, 7, 9, and may be found at ttp://dx.doi.org/10.1103/PhysRevMaterials.7.094002. Copyright 2023 American Physical Society

(Article begins on next page)

26 November 2026

Cluster charge-density-wave glass in hydrogen-intercalated $TiSe_2$

Giacomo Prando [1,*] Erik Piatti [2] Dario Daghero [2] Renato S. Gonnelli [2] and Pietro Carretta [1]
[1]Dipartimento di Fisica, Università degli Studi di Pavia, I-27100 Pavia, Italy
[2]Department of Applied Science and Technology, Politecnico di Torino, I-10129 Torino, Italy

(Received 16 May 2023; revised 24 July 2023; accepted 17 August 2023; published 5 September 2023)

The topotactic intercalation of transition-metal dichalcogenides with atomic or molecular ions acts as an efficient knob to tune the electronic ground state of the host compound. A representative material in this sense is $1T$-$TiSe_2$, where the electric-field-controlled intercalations of lithium or hydrogen trigger superconductivity coexisting with the charge-density-wave phase. Here, we use the nuclear magnetic moments of the intercalants in hydrogen-intercalated $1T$-$TiSe_2$ as local probes for nuclear magnetic resonance experiments. We argue that fluctuating mesoscopic-sized domains nucleate already at temperatures higher than the bulk critical temperature to the charge-density-wave phase and display cluster-glass-like dynamics in the MHz range tracked by ^{1}H nuclear moments. Additionally, we observe a well-defined independent dynamical process at lower temperatures that we associate with the intrinsic properties of the charge-density-wave state. In particular, we ascribe the low-temperature phenomenology to the collective phasonlike motion of the charge-density wave being hindered by structural defects and chemical impurities and resulting in a localized oscillating motion.

DOI: 10.1103/PhysRevMaterials.7.094002

I. INTRODUCTION

The wide range of electronic properties characterizing transition-metal dichalcogenides (TMDs) makes these materials remarkably interesting from both fundamental and application-oriented perspectives [1–5]. The representative chemical formula of TMDs is MX_2, where M and X are transition-metal and chalcogen elements, respectively. In spite of their vast chemical variety, TMDs share a common crystallographic structure resulting from the stacking of MX_2 trilayers. Each trilayer is composed of an atomically thin layer of M ions sandwiched between two closely packed layers made of X ions covalently bonded with the M ions [6]. The stacked trilayers interact among them via weak van-der-Waals–like forces, the covalent-bond-free interface between different trilayers being referred to as the van der Waals gap. As a result, TMDs can be conveniently exfoliated down to the single-trilayer, two-dimensional limit. The layered structure makes TMDs suitable hosts for topotactic intercalation with atomic or molecular ions as well as neutral molecules [7]. The interest for intercalated TMDs is their potential as solid ionic conductors [8–10] and, at the same time, the efficient control on the electronic properties of the host material offered by the intercalation [11–18].

A prototypal example in this sense is $1T$-$TiSe_2$. The pristine composition has been investigated extensively since the 1970s after the first reports of a commensurate $2\times2\times2$ charge-density-wave (CDW) state developing from a high-temperature semimetallic phase [19,20]. The historical relevance of this discovery, together with similar observations in other TMDs, was the departure from the then-accepted paradigm, due to Peierls, of the CDW transition being specific to one-dimensional systems simultaneously undergoing a metal-to-insulator phase transition—both aspects being violated in TMDs [21–29]. Although the transition temperature to the CDW phase is $T_{CDW} \sim 200$ K, a gap opening was reported in limited portions of the Fermi surface already at higher temperatures [30,31], consistent with the observation of higher transition temperatures to the CDW state in the single-trilayer limit [32–34]. The properties of the CDW phase in pristine $1T$-$TiSe_2$ are highly peculiar [35,36], and, almost 50 years after its first observation, the discussion on the main driving microscopic mechanism underlying such a state—electron-phonon coupling as opposed to exciton condensation—is still ongoing [37–50].

The electronic properties of the pristine $1T$-$TiSe_2$ composition can be tuned by physical and/or chemical means. Superconductivity with critical temperatures around a few Kelvins is triggered by pressure [51], electric-field-induced charge doping [52], and by intercalation using different atomic ions [53–55]. The CDW phase is suppressed by electric-field-induced charge doping [52], copper intercalation [53], and titanium self-doping [56]—however, the electric-field-controlled intercalation using lithium [54] and hydrogen [55] does not alter the T_{CDW} value estimated by means of electrical transport measurements. Remarkably, a structure of nanoscopic domains with alternating commensurate-incommensurate CDW phases emerges in $1T$-$TiSe_2$ when perturbed by electric fields or by the Li intercalation, the superconducting state being possibly confined to the incommensurate-CDW domains [52,54]. In spite of the detailed description of the spatial intertwining of different phases at low temperatures, a microscopic investigation of the high-temperature CDW state in the intercalated systems is still missing.

In this work, we use the magnetic moments of ^{1}H nuclei in hydrogen-intercalated $1T$-$TiSe_2$ as local probes for

*giacomo.prando@unipv.it

 ©2023 American Physical Society

nuclear magnetic resonance (NMR) experiments. Based on our modeling of the temperature dependence of the spin-lattice relaxation rate of the ^{1}H nuclear magnetization, we argue that a cluster CDW glass state is realized in the high-temperature limit, favored by the disordered configuration of the intercalants. Our evidence suggests that fluctuating mesoscopic-sized domains nucleate already at temperatures higher than T_{CDW}, slowing down towards a percolating CDW state throughout the sample and resulting in slow dynamics in the MHz range tracked by the ^{1}H nuclear moments. Additionally, we observe a well-defined independent dynamical process at lower temperatures that we associate with the intrinsic properties of the CDW state. In particular, we argue that the collective phasonlike motion of the CDW is hindered by structural defects and chemical impurities acting as pinning centers, resulting in a localized oscillating motion detected by the nuclear moments.

II. EXPERIMENTAL DETAILS AND RESULTS

We protonated flakelike $1T$-$TiSe_2$ single crystals (HQ Graphene) immersing them in a Duran crucible filled with 1-ethyl-3-methylimidazolium tetrafluoroborate (Sigma Aldrich) immediately after cleavage and applying a gate voltage 3 V between a platinum electrode and $1T$-$TiSe_2$ [55]. For this aim, the crystals were electrically contacted via a small droplet of silver paste (RS components). All the samples were gated in ambient atmosphere and at temperature $T = 300$ K, using the gating time as a knob to control the protonation state [55]. After the gating process, we thoroughly rinsed the crystals with acetone and ethanol and stored them in a vacuum dessicator.

We performed pulsed ^{1}H NMR experiments [57–61] at two fixed values of magnetic field ($\mu_0 H = 1.95$ and 3.46 T). The field was oriented parallel to the crystallographic *ab* planes of a collection of six stacked protonated $1T$-$TiSe_2$ crystals (gating time 60 min), each with approximate surface $\sim 2\times 2$ mm^2. We controlled the sample temperature with a dynamic continuous-flow cryostat using either liquid helium or liquid nitrogen, quantifying the temperature value using a thermocouple end close to the sample site. The data shown in the text belong to several cooling and warming cycles, and in order to maximize the reproducibility of the results, we always aimed at comparable thermal protocols. In particular, we cooled the sample in-field down to the lowest attainable temperature (depending on the cryogenic liquid being used) and settled the temperature on warming to perform each measurement.

We base all our results on the conventional inversion-recovery sequence of radiofrequency pulses shown in Fig. 1 (inset). The two $\pi/2$ pulses, with typical length ~ 1 μs and separated by $\tau_e \simeq 30$ μs, generate a solid echo at time τ_e after the second pulse. The sign and amplitude of the echo depend on the variable time τ between the inversion π pulse and the first $\pi/2$ pulse. For each τ value, the sequence is repeated and the signal cumulated until a satisfactory signal-to-noise ratio is achieved. The second half of the echo signal is fast-Fourier-transformed and the integral I of the transform is reported as a function of τ to obtain the time recovery of the nuclear magnetization towards the state of thermal equilibrium—see Fig. 1 for representative data. In the case of spin-1/2 nuclei,

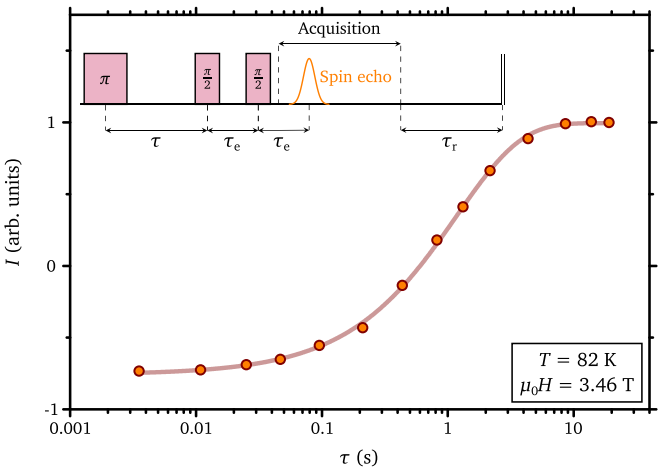

FIG. 1. Representative recovery of the ^{1}H nuclear magnetization towards the thermodynamic equilibrium as a function of the time τ elapsed between the π pulse and the first $\pi/2$ pulse. I represents the integral of the fast-Fourier-transformed echo shown later in the inset to Fig. 2. The continuous line is a best-fitting function according to Eq. (1). The inset shows a scheme of the pulsed inversion sequence used to perform the measurements discussed throughout the text (time durations are not in proportion).

the expected recovery for the nuclear magnetization M is purely exponential according to the following function [60]:

$$M(\tau) = M(0) + \Delta M \left\{1 - \exp\left[-\left(\frac{\tau}{T_1}\right)^{\beta}\right]\right\} \qquad (1)$$

from which the spin-lattice relaxation time T_1 is quantified. The fitting function in Eq. (1) accounts for possible deviations of the pulse lengths from their ideal values, resulting in an imperfect initial inversion of the nuclear magnetization. Also, Eq. (1) accounts for possible deviations from the expected exponential behavior through the empirical stretching parameter β, thus accounting for nonhomogeneous local environments probed by the nuclei. Finally, the fast-Fourier-transformed echo for the longest τ value, i.e., such that the thermal equilibrium is attained, is fitted using an empirical Gaussian function

$$y = \frac{A}{w}\sqrt{\frac{2}{\pi}} \exp\left[-2\left(\frac{\nu - \nu_L}{w}\right)^2\right] \qquad (2)$$

in order to quantify the linewidth w—see the inset to Fig. 2 for representative data (ν_L is the Larmor frequency and A is the subtended area). Importantly, the repetition time τ_r is calibrated in every measurement so that $\tau_r \gtrsim 5T_1$ to allow the nuclear magnetization to reach the equilibrium state before starting the pulsed sequence over again.

We report the dependence of the spectral width w on temperature in Fig. 2. The linewidth is approximately constant below ~ 240 K and it sharply gets much narrower at higher temperatures. In spite of the sizable error bars, it is possible to detect a weak, field-independent increase of the linewidth upon cooling the sample below ~ 100 K. The dependence of $1/T_1$ on temperature is shown in Fig. 3 for the two values of magnetic field. Although not shown explicitly, the stretching parameter takes values $\beta \simeq 0.9 \pm 0.05$ within the whole

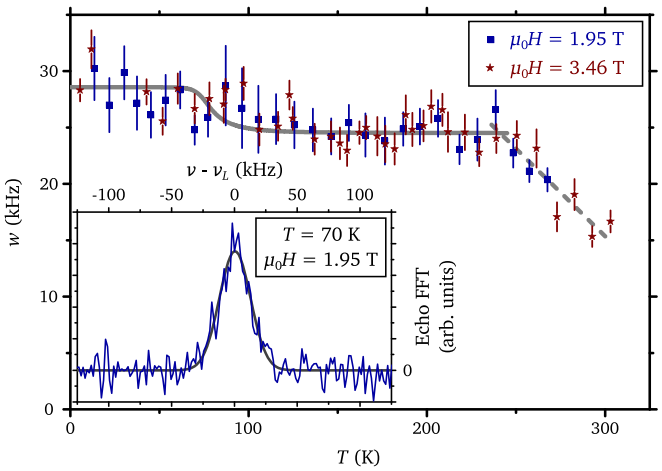

FIG. 2. Inset: the blue curve is the fast Fourier transform (FFT) of a representative echo signal at long recovery times. The black curve is a best-fitting of the data using the function in Eq. (2). Main panel: dependence of the spectral width on temperature. The continuous line is obtained from Eq. (6) (see the discussion later on in the text). The dashed line is a guide to the eye.

investigated temperature window without any detectable trend. As prominent features, we notice a local maximum at around 70 K followed by a marked peak at around 180 K. The amplitude as well as the position of these peaks are dependent on the magnetic field. In spite of the comparable thermal protocols used to perform our measurements, we stress that the spin-lattice relaxation rate shows effects of thermal history, as highlighted in the inset to Fig. 3. In the following analysis, we will refer to the lower branch (red stars) because of an overall agreement shown between cooling cycles using liquid nitrogen and helium (with the exception of one specific cooling cycle using liquid nitrogen, denoted with yellow stars).

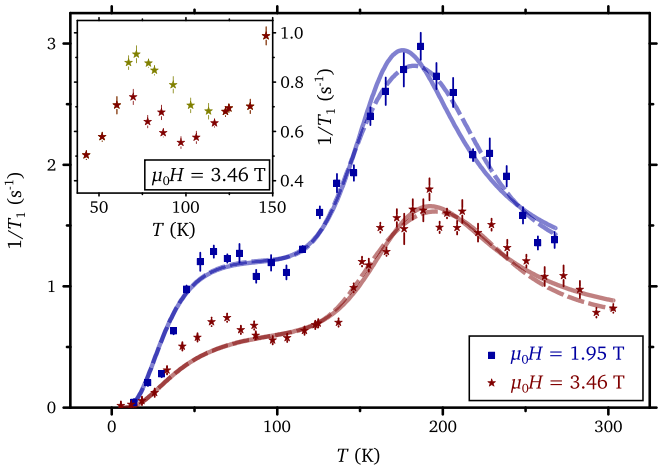

FIG. 3. Main panel: dependence of the spin-lattice relaxation rate on temperature at different values of the magnetic field. The continuous lines are the results of a global curve fitting based on Eq. (5). The dashed lines are the results of a global curve fitting based on Eq. (5) assuming a flat distribution for the activation temperature $\vartheta_{\rm HT}$—see Eq. (A5). Inset: thermal-history effects on the spin-lattice relaxation rate observed for different cooling runs.

III. MODELING THE SPIN-LATTICE RELAXATION RATE

The nuclear spin-lattice relaxation rate is proportional to the spectral density $J(\omega_L)$ of the fluctuating local magnetic field at the nuclear site in the directions orthogonal to the quantization axis, and calculated at the Larmor angular frequency $\omega_L = 2\pi\nu_L$ [57,60]. Assuming that the autocorrelation function for the fluctuations of the local field is an exponentially decaying function leads to a conventional Lorentzian functional form for the spectral density [62]

$$J(\omega) = \frac{\tau_c}{1+\omega^2\tau_c^2} \tag{3}$$

governed by the correlation time τ_c characterizing the dynamics. In the particular case of the relaxation being driven by the time modulation of the nuclear dipole-dipole interaction, the following Kubo-Tomita (KT) formula is valid for the spin-lattice relaxation rate [57,63]:

$$T_1^{-1}(T)^{\rm KT} = C[J(\omega_L) + 4\,J(2\omega_L)], \tag{4}$$

where the factor $C \sim \gamma^2\langle\Delta B^2\rangle$ includes the mean-square amplitude of the transverse fluctuating field ΔB and the proton gyromagnetic ratio γ. Accordingly, we write

$$T_1^{-1}(T) = T_1^{-1}(T)^{\rm KT}_{\rm LT} + T_1^{-1}(T)^{\rm KT}_{\rm HT} \tag{5}$$

to account for the two independent processes observed at low and high temperature in the experimental data (LT and HT, respectively). Assuming $\tau_{c,\rm LT} = \tau_{0,\rm LT}\exp(\vartheta_{\rm LT}/T)$ and $\tau_{c,\rm HT} = \tau_{0,\rm HT}\exp(\vartheta_{\rm HT}/T)$, i.e., an Arrhenius-like dependence on temperature for both the correlation times with activation temperatures $\vartheta_{\rm LT}$ and $\vartheta_{\rm HT}$, gives us a fitting function to describe the experimental data in Fig. 3.

The results of a global data fitting based on Eq. (5), sharing all the fitting parameters except the Larmor frequencies between the two data sets, are shown in the main panel of Fig. 3 as continuous lines. The numerical results of the fitting parameters are reported in Table I. The agreement with the experimental data is satisfactory in spite of the deviation observed for $T \lesssim 80$ K for the high-field data. We stress that the slowing down of a time-modulated nuclear dipole-dipole interaction should be reflected in an extra broadening of the spectral linewidth upon decreasing temperature based on the expression [57]

$$w^2 = \frac{2w_0^2}{\pi}\arctan(\pi\, w\,\tau_c), \tag{6}$$

where w_0 is the rigid-lattice linewidth. We solved Eq. (6) using the fitting parameters estimated from the global-fitting procedure described above and, in particular, the numerical values defining $\tau_{c,\rm HT}$. The result is shown by the continuous line in the main panel of Fig. 2. In spite of the sizable error bars, the experimental data are consistent with the expected trend. A similar increase in the linewidth is expected at even lower temperatures based on Eq. (6) using $\tau_{c,\rm LT}$—however, our experimental data at low temperatures are not dense enough to resolve the expected behavior.

The quality of the global fitting in the main panel of Fig. 3 can be improved by assuming a statistical distribution of correlation times $\tau_{c,\rm HT}$. For this aim, a straightforward way to proceed is to assume a well-defined value for $\tau_{0,\rm HT}$ and a flat, square distribution of activation energies $\vartheta_{\rm HT}$ extended

TABLE I. Results of the fitting procedures based on Eqs. (5) and (A5) for the $1/T_1$ data shown in Figs. 3 and 4.

	C_{LT} (10^8 s^{-2})	$\tau_{0,\mathrm{LT}}$ (10^{-10} s)	ϑ_{LT} (K)	C_{HT} (10^8 s^{-2})	$\tau_{0,\mathrm{HT}}$ (10^{-13} s)	ϑ_{HT} (K)	$\delta\vartheta_{\mathrm{HT}}$ (K)
Current sample	4.4 ± 0.1	6.1 ± 0.2	65 ± 1	6.5 ± 0.1	12 ± 1	1210 ± 20	0 (fixed)
	4.4 ± 0.1	6.2 ± 0.2	65 ± 1	8.3 ± 0.2	1.2 ± 0.1	1650 ± 10	320 ± 20
Sample from Ref. [55]	41.2 ± 0.4	0.59 ± 0.01	24.0 ± 0.5	15 ± 1	13 ± 5	1040 ± 60	350 ± 30

over the window $(\vartheta_{\mathrm{HT}} - \delta\vartheta_{\mathrm{HT}}, \vartheta_{\mathrm{HT}} + \delta\vartheta_{\mathrm{HT}})$. The analytical result is derived in Appendix A. Plugging Eq. (A5) for the HT process in Eq. (5) and repeating the global data fitting results in the dashed lines in Fig. 3. The numerical results of the fitting parameters are reported in Table I.

IV. DISCUSSION

Based on the results reported in Ref. [55], we expect different possible microscopic intercalation sites for hydrogen in $1T$-$TiSe_2$—i.e., within the van der Waals gap and inside the trilayers—as well as multiple microscopic configurations for the intercalants. In particular, we expect regions with occupied intercalation sites as well as regions without intercalants—at the same time, Raman spectroscopy evidences a partial intercalation of molecular hydrogen [55].

Overall, hydrogen is intercalated in a highly disordered configuration, which leads to a single spectral contribution in our NMR measurements, as highlighted in the inset to Fig. 2. Still, the dependence of the spectral linewidth on temperature is still highly instructive. In particular, we interpret the sharp decrease of the spectral linewidth upon increasing temperature above ~240 K as a motional-narrowing effect associated with the diffusion of the intercalated hydrogen ions. More precisely, we argue that the condition $2\pi w\tau_c^{\mathrm{diff}} \gg 1$ (i.e., $\tau_c^{\mathrm{diff}} \gg 5$ μs) is satisfied for $T \lesssim 240$ K, where τ_c^{diff} is the correlation time characteristic of the hydrogen diffusion throughout the lattice. To reinforce our interpretation, we notice that our results are in perfect qualitative agreement with previous continuous-wave NMR measurements on hydrogen-intercalated $1T$-TiS_2 [64]. This latter material is of particular importance for our aims since it is isostructural to $1T$-$TiSe_2$ and, interestingly, it does not show any transition to a CDW phase. Based on these arguments, we safely conclude that the hydrogen ions form a rigid lattice integral with the $1T$-$TiSe_2$ host crystal lattice for $T \lesssim 240$ K, i.e., where we observe all the features that we are going to discuss below.

Before proceeding with the interpretation of our data, it is interesting to compare the current results with the dependence of $1/T_1$ on temperature at $\mu_0 H = 3.46$ T reported previously in Ref. [55] for another collection of stacked protonated $1T$-$TiSe_2$ crystals (gating time 30 min—see Fig. 4). Our previous interpretation of those data was based on the Korringa-like linear trend between 80 and 170 K, suggesting that the deviations at higher temperatures could be due to a reconstruction of the Fermi surface resulting from the CDW state onset [55]. Such an interpretation was motivated by the observation of generalized Korringa trends both in pristine, isotopically enriched $TiSe_2$ measured by ^{77}Se NMR [65] as well as in other TMDs such as VSe_2, VS_2, and $IrTe_2$ [66–68]. The additional marked peak at lower temperature was reported for pristine $TiSe_2$ as well [65]—although its origin has remained, to the best of our knowledge, elusive [69]—clearly suggesting that our ^{1}H NMR measurements are directly probing the intrinsic dynamics of $TiSe_2$. However, at this stage, the new currently discussed results urge us to reinterpret all the data within the same model. In particular, it is clear that the spin-lattice relaxation rate should be described for all the samples in terms of two well-defined maxima located at low and high temperatures, respectively, the latter seemingly correlating with T_{CDW}. The result of a best-fitting procedure based on Eqs. (5) and (A5), again assuming a flat distribution of correlation times for the HT process, is reported as a dashed line in Fig. 4 (and the resulting fitting parameters in Table I) showing a satisfactory agreement with the experimental data. In spite of the major quantitative differences between the two samples, we argue that the underlying mechanisms leading to the spin-lattice relaxation are the same.

A. High-temperature peak

We focus on the $T \gtrsim 100$ K limit first. In spite of the limited amount of experimental data, the results for pristine $TiSe_2$ in Ref. [65] do not highlight any well-defined maximum in the spin-lattice relaxation rate for $T \gtrsim 100$ K, thus suggesting that the currently observed feature is specific to the hydrogen-intercalated system. The broad shape of the temperature dependence of $1/T_1$, together with the characteristic dependence on the magnetic field, suggest that the origin of the observed maximum should not be associated with any critical dynamics. Consistently with the observation

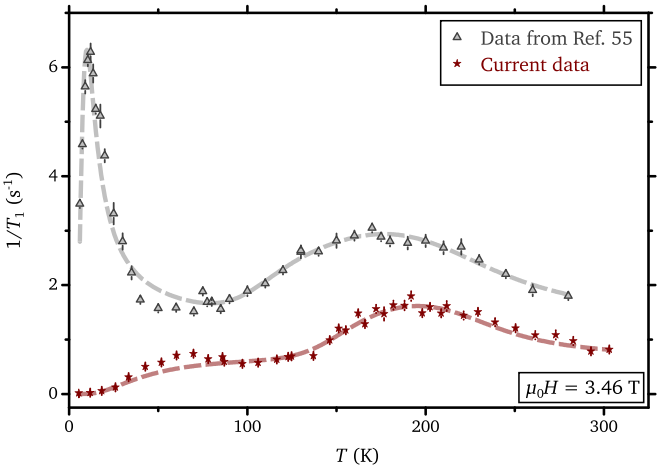

FIG. 4. Dependence of the spin-lattice relaxation rate on temperature at $\mu_0 H = 3.46$ T for the current sample (red stars, same data as in Fig. 3) and for another hydrogen-intercalated $TiSe_2$ sample measured previously (gray triangles, data from Ref. [55]). The dashed lines are the best-fitting curves based on Eqs. (5) and (A5), assuming a statistical distribution of correlation times only for the activation temperature ϑ_{HT} (the red curve is the same as in Fig. 3).

on the narrowing of the spectral linewidth, it is unrealistic to associate such dynamics with the diffusion of the intercalated ions as, based on our comments above, the condition $1/\tau_c^{\rm diff} \ll \omega_L$ is satisfied at least up to ∼240 K. Consistently with these arguments, we stress that several systems with a comparable structure and chemical formula show diffusion-related maxima in $1/T_1$ at higher temperatures if compared to our observations [70–76].

In light of the arguments above, it is a natural assumption that the—presumably sample-dependent—intrinsic disorder associated with the intercalation process is reflected in a short-range-ordered CDW phase [77,78]. Here, the order is confined within correlated mesoscopic islands lacking phase coherence among themselves at high temperatures until long-range order is recovered for $T \lesssim T_{\rm CDW}$. The slow dynamics of the disordered state, corresponding to a CDW glass [79] or—more precisely—cluster glass, results in a noncritical peak in the spin-lattice relaxation rate consistent with our observations [80,81]. The persistence of the contribution to $1/T_1$ at temperatures well above $T_{\rm CDW}$ could imply that the intercalation process favors the insurgence of a segregated, preemptive CDW state at high temperatures, amplifying the tendency of the system towards the order implied by the partial gap opening for $T \gg T_{\rm CDW}$ [30,31].

Within this scenario, two different mechanisms can be identified in order to justify the relaxation mechanism for the nuclear ensemble. On the one hand, the dynamics of the CDW clusters would induce a slow, noncritical local dynamics of the lattice and of the intercalated hydrogen ions, in turn. In this view, a conventional nuclear dipole-dipole relaxation among the intercalated ions would be induced and drive the spin-lattice relaxation—thus justifying the use of Eq. (4) above. Another possible mechanism is the time modulation of the Knight shift distribution induced by the CDW state [82,83]. The lack of any dependence of the extra linewidth broadening for $T \lesssim 150$ K on the magnetic field (see Fig. 2) seems to rule out the latter mechanism in favor of the nuclear dipole-dipole relaxation.

B. Low-temperature peak

We now focus on the peak in $1/T_1$ observed for $T \lesssim 100$ K in Figs. 3 and 4. As mentioned above, this maximum as well as a frequency-dependent anomaly in the internal friction were observed in the same temperature range in pristine $TiSe_2$ [65,84,85]. This is a strong hint that the phenomenology observed by our experiments is not induced by the hydrogen intercalation but that it should rather be related to the intrinsic electronic properties of $1T$-$TiSe_2$. Another interesting observation comes from copper-intercalated Cu_xTiSe_2. It is well known that increasing the amount of intercalated copper acts as an efficient knob to progressively weaken the CDW state until its full suppression for $x \simeq 0.06$ while superconductivity develops for $x \gtrsim 0.04$ [53]. That said, it is remarkable that the spin-lattice relaxation rate measured by ^{77}Se NMR in two Cu_xTiSe_2 samples where the CDW state is strongly suppressed or even absent only shows a well-defined Korringa-like linear dependence on temperature over the entire accessed range down to low temperatures [86]. Associating the well-defined low-temperature peak in $1/T_1$ with the intrinsic properties of the CDW is consistent with this latter observation. We stress that the local detection of intrinsic CDW features at the hydrogen site confirms that the phase segregation of CDW-ordered, hydrogen-poor regions and superconducting, hydrogen-rich regions—with progressive volume redistribution within the two as the protonation time increases—is not the correct model to describe the state realized by the intercalation, as already argued in [55].

Having excluded that the low-temperature maximum in $1/T_1$ arises from a change in the electronic structure or from the onset of magnetism [19,55,65,87,88], a possible explanation for our results is that the spin-lattice relaxation is influenced by the low-frequency dynamics of the CDW itself. Indeed, the collective excitations of the CDW state (i.e., phase modes and amplitude modes) can influence the spin-lattice relaxation [89–91]—however, some words of caution are in order. The vast majority of the results have been obtained using quadrupolar nuclei that couple directly with the local electric-field gradients and lattice distortions generated by the CDW state [92–98]. In our current case of ^{1}H-NMR, we argue that the mechanism underlying the spin-lattice relaxation is due to a time-modulated nuclear dipole-dipole interaction due to a time-modulated lattice distortion induced by the CDW dynamics (see above).

At the same time, it is well known that collective phase-mode excitations are not free to slip throughout the system in the case of a commensurate CDW state [91] akin to the one realized in $TiSe_2$, where the lattice is particularly efficient in pinning the spatial modulation of the charge. For this reason, we assume that the CDW state is localized but still able to oscillate around its equilibrium position as a result of thermal excitations. In this case, the time-dependent oscillations of the CDW can induce an efficient relaxation when the characteristic correlation time of the dynamics matches the inverse of the Larmor frequency. We expect that this phenomenology is strongly influenced by the level (and, more in general, the strength) of impurities, structural defects, and disorder in the system [77,99–102], acting as pinning centers for the CDW state. Both the sample-dependent position and amplitude of the low-temperature peak as well as the observation of clear thermal-history hysteretic effects are consistent with this expectation [103]. Based on this interpretation, the observation of a higher $\vartheta_{\rm HT}$ value for the current data—if compared to the results reported in Ref. [55]—suggest that the currently investigated sample contains a much higher degree of impurities and structural defects. This expectation is seemingly confirmed by the dependence of the electrical resistivity (ρ) on temperature (see Ref. [55]) and by the residual resistivity ratio (RRR), $\rho(295\ {\rm K})/\rho_0$, characteristic of the two samples (ρ_0 being the residual resistivity just before superconductivity sets in). RRR $\simeq 9.3$ for the current sample, while RRR $\simeq 12.1$ for the sample studied in Ref. [55], consistently with a lower degree of impurities and defects in the latter case.

V. SUMMARIZING REMARKS AND CONCLUSIONS

We discussed the results of ^{1}H nuclear magnetic resonance experiments on hydrogen-intercalated $TiSe_2$ crystals. In this system, the intercalation induces robust and nonvolatile

superconductivity, as shown in Ref. [55]. Our current results suggest that the disorder associated with the intercalation induces an inhomogeneous charge-density-wave phase. In particular, we argue that stable mesoscopic charge-density-wave-ordered regions lacking phase coherence among them nucleate already at temperatures higher than the bulk transition temperature T_{CDW}. The noncritical dynamics of this cluster-glass charge-density-wave state influences the spin-lattice relaxation of the ^{1}H nuclear magnetization, showing a well-defined Kubo-Tomita-like trend with a characteristic dependence on temperature and on the magnetic field. Additionally, we reported clear evidence of an additional anomaly in the spin-lattice relaxation rate at low temperatures akin to what was reported for the pristine $TiSe_2$ composition in Ref. [65] and whose origin should be related to the intrinsic properties of the charge-density-wave phase. The low-temperature dynamics is strongly sample-dependent and is likely associated with the complicated interplay of the charge-density-wave state with pinning centers such as impurities and structural defects. Further complementary insights into the charge-density-wave dynamics could be obtained performing ^{7}Li nuclear magnetic resonance experiments on lithiated $TiSe_2$, exploiting the nonvanishing quadrupole moment of ^{7}Li nuclei and its direct coupling to local electric-field gradients and lattice distortions generated by the charge-density-wave phase.

ACKNOWLEDGMENTS

We acknowledge insightful discussions with F. Borsa and A. Rigamonti. We are grateful to S. Roddaro for providing us with the pristine $TiSe_2$ crystals. We thank S. Resmini for support during the NMR measurements. G.P. acknowledges support by the PNRR MUR project PE0000023-NQSTI. E.P., D.D., and R.S.G. acknowledge support from the MIUR PRIN-2017 program (Grant No. 2017Z8TS5B Tuning and understanding Quantum phases in 2D materials Quantum2D).

APPENDIX: GENERALIZATION OF THE KUBO-TOMITA EXPRESSION IN THE PRESENCE OF A CONSTANT DISTRIBUTION OF ACTIVATION TEMPERATURES

The well-known Kubo-Tomita expression for the spin-lattice relaxation induced by the nuclear dipole-dipole interaction can be written as follows [63]:

$$\frac{1}{T_1} = C\left(\frac{\tau_c}{1+\omega_L^2\tau_c^2} + \frac{4\tau_c}{1+4\omega_L^2\tau_c^2}\right) \tag{A1}$$

with contributions from the spectral density $J(\omega)$ for the fluctuations of the local magnetic field perpendicular to the quantization axis calculated at ω_L and $2\omega_L$. Assuming an Arrhenius-like temperature dependence for the correlation time $\tau_c = \tau_0 \exp(\vartheta/T)$ and substituting in Eq. (A1), it is straightforward to show that

$$\frac{1}{T_1} = \frac{C}{2\omega_L}\left\{\left[\cosh\left(\frac{\vartheta}{T} + \ln(\omega_L\tau_0)\right)\right]^{-1} + 2\left[\cosh\left(\frac{\vartheta}{T} + \ln(2\omega_L\tau_0)\right)\right]^{-1}\right\}. \tag{A2}$$

The effect of a distribution of correlation times (and, in particular, of activation energies) can be accounted for by considering the expression

$$\frac{1}{T_1} = \frac{C}{2\omega_L}\int_{-\infty}^{+\infty}\left\{\left[\cosh\left(\frac{\Delta}{T} + \ln(\omega_L\tau_0)\right)\right]^{-1} + 2\left[\cosh\left(\frac{\Delta}{T} + \ln(2\omega_L\tau_0)\right)\right]^{-1}\right\}p(\Delta)d\Delta, \tag{A3}$$

where $p(\Delta)$ is a normalized probability distribution function. An approximated but convenient choice is that of a constant distribution such that $p(\Delta) = 1/(2\delta\vartheta)$ for $\vartheta - \delta\vartheta < \Delta < \vartheta + \delta\vartheta$ [and $p(\Delta) = 0$ elsewhere]. Consequently,

$$\frac{1}{T_1} = \frac{C}{4\omega_L\delta\vartheta}\int_{\vartheta-\delta\vartheta}^{\vartheta+\delta\vartheta}\left\{\left[\cosh\left(\frac{\Delta}{T} + \ln(\omega_L\tau_0)\right)\right]^{-1} + 2\left[\cosh\left(\frac{\Delta}{T} + \ln(2\omega_L\tau_0)\right)\right]^{-1}\right\}d\Delta, \tag{A4}$$

which is solved as

$$\frac{1}{T_1} = \frac{C\,T}{4\omega_L\delta\vartheta}\left\{\arctan\left[\sinh\left(\frac{\vartheta+\delta\vartheta}{T} + \ln(\omega_L\tau_0)\right)\right] - \arctan\left[\sinh\left(\frac{\vartheta-\delta\vartheta}{T} + \ln(\omega_L\tau_0)\right)\right] + 2\arctan\left[\sinh\left(\frac{\vartheta+\delta\vartheta}{T} + \ln(2\omega_L\tau_0)\right)\right] - 2\arctan\left[\sinh\left(\frac{\vartheta-\delta\vartheta}{T} + \ln(2\omega_L\tau_0)\right)\right]\right\}. \tag{A5}$$

[1] B. Radisavljevic, A. Radenovic, J. Brivio, V. Giacometti, and A. Kis, Single-layer MoS_2 transistors, Nat. Nanotechnol. **6**, 147 (2011).

[2] Q. H. Wang, K. Kalantar-Zadeh, A. Kis, J. N. Coleman, and M. S. Strano, Electronics and optoelectronics of two-dimensional transition metal dichalcogenides, Nat. Nanotechnol. **7**, 699 (2012).

[3] A. Geim and I. Grigorieva, Van der Waals heterostructures, Nature **499**, 419 (2013).

[4] F. H. L. Koppens, T. Mueller, P. Avouris, A. C. Ferrari, M. S. Vitiello, and M. Polini, Photodetectors based on graphene, other two-dimensional materials and hybrid systems, Nat. Nanotechnol. **9**, 780 (2014).

[5] S. Manzeli, D. Ovchinnikov, D. Pasquier, O. V. Yazyev, and A. Kis, 2D transition metal dichalcogenides, Nat. Rev. Mater. **2**, 17033 (2017).

[6] J. A. Wilson and A. D. Yoffe, The transition metal dichalcogenides. Discussion and interpretation of the observed optical,

electrical and structural properties, Adv. Phys. **18**, 193 (1969).

[7] *Intercalation in Layered Materials*, edited by M. S. Dresselhaus (Springer, New York, 1986).

[8] M. S. Whittingham, Chemistry of intercalation compounds: metal guests in chalcogenide hosts, Prog. Solid State Chem. **12**, 41 (1978).

[9] I. Samaras, S. I. Saikh, C. Julien, and M. Balkanski, Lithium insertion in layered materials as battery cathodes, Mater. Sci. Eng.: B **3**, 209 (1989).

[10] A. V. Powell, Intercalation compounds of low-dimensional transition metal chalcogenides, Annu. Rep. Prog. Chem. Sect. C **90**, 177 (1993).

[11] S. S. P. Parkin and R. H. Friend, 3d transition-metal intercalates of the niobium and tantalum dichalcogenides. I. Magnetic properties, Philos. Mag. B **41**, 65 (1979).

[12] R. H. Friend and A. D. Yoffe, Electronic properties of intercalation complexes of the transition metal dichalcogenides, Adv. Phys. **36**, 1 (1987).

[13] R. A. Klemm, Pristine and intercalated transition metal dichalcogenide superconductors, Physica C **514**, 86 (2015).

[14] D. Voiry, A. Mohite, and M. Chhowalla, Phase engineering of transition metal dichalcogenides, Chem. Soc. Rev. **44**, 2702 (2015).

[15] R. Wang, Y. Yu, S. Zhou, H. Li, H. Wong, Z. Luo, L. Gan, and T. Zhai, Strategies on phase control in transition metal dichalcogenides, Adv. Funct. Mater. **28**, 1802473 (2018).

[16] Y. Li, H. Yan, B. Xu, L. Zhen, and C.-Y. Xu, Electrochemical intercalation in atomically thin van der Waals materials for structural phase transition and device applications, Adv. Mater. **33**, 2000581 (2021).

[17] M. Wang, S. Xu, and J. J. Cha, Revisiting intercalation-induced phase transitions in 2D group VI transition metal dichalcogenides, Adv. Energy Sustain. Res. **2**, 2100027 (2021).

[18] J.-B. Vaney, B. Vignolle, A. Demourgues, E. Gaudin, E. Durand, C. Labrugère, A. Bernardini, F. Cano, and S. Tencé, Topotactic fluorination of intermetallics as an efficient route towards quantum materials, Nat. Commun. **13**, 1462 (2022).

[19] F. J. Di Salvo, D. E. Moncton, and J. V. Waszczak, Electronic properties and superlattice formation in the semimetal $TiSe_2$, Phys. Rev. B **14**, 4321 (1976).

[20] J. C. E. Rasch, T. Stemmler, B. Müller, L. Dudy, and R. Manzke, 1T-$TiSe_2$: Semimetal or Semiconductor?, Phys. Rev. Lett. **101**, 237602 (2008).

[21] R. E. Peierls, *Quantum Theory of Solids* (Oxford University Press, Oxford, 1955).

[22] F. J. Di Salvo and T. M. Rice, Charge-density waves in transition-metal compounds, Phys. Today **32**(5), 32 (1979).

[23] R. V. Coleman, B. Giambattista, P. K. Hansma, A. Johnson, W. W. McNairy, and C. G. Slough, Scanning tunnelling microscopy of charge-density waves in transition metal chalcogenides, Adv. Phys. **37**, 559 (1988).

[24] G. Grüner, The dynamics of charge-density waves, Rev. Mod. Phys. **60**, 1129 (1988).

[25] R. E. Thorne, Charge-density-wave conductors, Phys. Today **49**(5), 42 (1996).

[26] J. A. Wilson, F. J. Di Salvo, and S. Mahajan, Charge-density waves and superlattices in the metallic layered transition metal dichalcogenides, Adv. Phys. **50**, 1171 (2001).

[27] G. Li, W. Z. Hu, D. Qian, D. Hsieh, M. Z. Hasan, E. Morosan, R. J. Cava, and N. L. Wang, Semimetal-to-Semimetal Charge Density Wave Transition in 1T-$TiSe_2$, Phys. Rev. Lett. **99**, 027404 (2007).

[28] P. Monceau, Electronic crystals: an experimental overview, Adv. Phys. **61**, 325 (2012).

[29] X. Zhu, J. Guo, J. Zhang, and E. W. Plummer, Misconceptions associated with the origin of charge density waves, Adv. Phys. X **2**, 622 (2017).

[30] Y. Miyahara, H. Bando, and H. Ozaki, Tunnelling spectroscopic study of the CDW energy gap in $TiSe_2$, J. Phys.: Condens. Matter **7**, 2553 (1995).

[31] P. Chen, Y.-H. Chan, X.-Y. Fang, S.-K. Mo, Z. Hussain, A.-V. Fedorov, M. Y. Chou, and T.-C. Chiang, Hidden order and dimensional crossover of the charge density waves in $TiSe_2$, Sci. Rep. **6**, 37910 (2016).

[32] P. Goli, J. Khan, D. Wickramaratne, R. K. Lake, and A. A. Balandin, Charge density waves in exfoliated films of van der Waals materials: evolution of Raman spectrum in $TiSe_2$, Nano Lett. **12**, 5941 (2012).

[33] P. Chen, Y.-H. Chan, X.-Y. Fang, Y. Zhang, M. Y. Chou, S.-K. Mo, Z. Hussain, A.-V. Fedorov, and T.-C. Chiang, Charge density wave transition in single-layer titanium diselenide, Nat. Commun. **6**, 8943 (2015).

[34] K. Sugawara, Y. Nakata, R. Shimizu, P. Han, T. Hitosugi, T. Sato, and T. Takahashi, Unconventional charge-density-wave transition in monolayer 1T-$TiSe_2$, ACS Nano **10**, 1341 (2016).

[35] J. Ishioka, Y. H. Liu, K. Shimatake, T. Kurosawa, K. Ichimura, Y. Toda, M. Oda, and S. Tanda, Chiral Charge-Density Waves, Phys. Rev. Lett. **105**, 176401 (2010).

[36] S.-Y. Xu, Q. Ma, Y. Gao, A. Kogar, A. Zong, A. M. Mier Valdivia, T. H. Dinh, S.-M. Huang, B. Singh, C.-H. Hsu, T.-R. Chang, J. P. C. Ruff, K. Watanabe, T. Taniguchi, H. Lin, G. Karapetrov, D. Xiao, P. Jarillo-Herrero, and N. Gedik, Spontaneous gyrotropic electronic order in a transition-metal dichalcogenide, Nature **578**, 545 (2020).

[37] B. I. Halperin and T. M. Rice, Possible anomalies at a semimetal-semiconductor transition, Rev. Mod. Phys. **40**, 755 (1968).

[38] B. I. Halperin and T. M. Rice, The excitonic state at the semiconductor-semimetal transition, Solid State Phys. **21**, 115 (1968).

[39] H. P. Hughes, Structural distortion in $TiSe_2$ and related materials - a possible Jahn-Teller effect?, J. Phys. C **10**, L319 (1977).

[40] R. M. White and G. Lucovsky, Suppression of antiferroelectricity in $TiSe_2$ by excess carriers, Il Nuovo Cimento B **38**, 280 (1977).

[41] J. A. Wilson, Concerning the semimetallic characters of TiS_2 and $TiSe_2$, Solid State Commun. **22**, 551 (1977).

[42] J. H. Gaby, B. DeLong, F. C. Brown, R. Kirby, and F. Lévy, Origin of the structural transition in $TiSe_2$, Solid State Commun. **39**, 1167 (1981).

[43] M. Holt, P. Zschack, H. Hong, M. Y. Chou, and T.-C. Chiang, X-Ray Studies of Phonon Softening in $TiSe_2$, Phys. Rev. Lett. **86**, 3799 (2001).

[44] T. E. Kidd, T. Miller, M. Y. Chou, and T.-C. Chiang, Electron-Hole Coupling and the Charge Density Wave Transition in $TiSe_2$, Phys. Rev. Lett. **88**, 226402 (2002).

[45] K. Rossnagel, L. Kipp, and M. Skibowski, Charge-density-wave phase transition in 1T-$TiSe_2$: Excitonic insulator versus

band-type Jahn-Teller mechanism, Phys. Rev. B **65**, 235101 (2002).

[46] A. Kogar, M. S. Rak, S. Vig, A. A. Husain, F. Flicker, Y. I. Joe, L. Venema, G. J. MacDougall, T. C. Chiang, E. Fradkin, J. van Wezel, and P. Abbamonte, Signatures of exciton condensation in a transition metal dichalcogenide, Science **358**, 1314 (2017).

[47] A. Wegner, J. Zhao, J. Li, J. Yang, A. A. Anikin, G. Karapetrov, K. Esfarjani, D. Louca, and U. Chatterjee, Evidence for pseudo-Jahn-Teller distortions in the charge density wave phase of 1T-$TiSe_2$, Phys. Rev. B **101**, 195145 (2020).

[48] M. R. Otto, J.-H. Pöhls, L. P. R. de Cotret, M. J. Stern, M. Sutton, and B. J. Siwick, Mechanisms of electron-phonon coupling unraveled in momentum and time: The case of soft phonons in $TiSe_2$, Sci. Adv. **7**, eabf2810 (2021).

[49] Z. Lin, C. Wang, A. Balassis, J. P. Echeverry, A. S. Vasenko, V. M. Silkin, E. V. Chulkov, Y. Shi, J. Zhang, J. Guo, and X. Zhu, Dramatic Plasmon Response to the Charge-Density-Wave Gap Development in 1T-$TiSe_2$, Phys. Rev. Lett. **129**, 187601 (2022).

[50] D. Novko, Z. Torbatian, and I. Lončarič, Electron correlations rule the phonon-driven instability in single-layer $TiSe_2$, Phys. Rev. B **106**, 245108 (2022).

[51] A. F. Kusmartseva, B. Sipos, H. Berger, L. Forró, and E. Tutiš, Pressure Induced Superconductivity in Pristine 1T-$TiSe_2$, Phys. Rev. Lett. **103**, 236401 (2009).

[52] L. J. Li, E. C. T. O'Farrell, K. P. Loh, B. Özyilmaz, and A. H. Castro Neto, Controlling many-body states by the electric-field effect in a two-dimensional material, Nature **529**, 185 (2016).

[53] E. Morosan, H. W. Zandbergen, B. S. Dennis, J. W. G. Bos, Y. Onose, T. Klimczuk, A. P. Ramirez, N. P. Ong, and R. J. Cava, Superconductivity in Cu_xTiSe_2, Nat. Phys. **2**, 544 (2006).

[54] M. Liao, H. Wang, Y. Zhu, R. Shang, M. Rafique, L. Yang, H. Zhang, D. Zhang, and Q.-K. Xue, Coexistence of resistance oscillations and the anomalous metal phase in a lithium intercalated $TiSe_2$ superconductor, Nat. Commun. **12**, 5342 (2021).

[55] E. Piatti, G. Prando, M. Meinero, C. Tresca, M. Putti, S. Roddaro, G. Lamura, T. Shiroka, P. Carretta, G. Profeta, D. Daghero, and R. S. Gonnelli, Superconductivity induced by gate-driven hydrogen intercalation in the charge-density-wave compound 1T-$TiSe_2$, Commun. Phys. **6**, 202 (2023).

[56] T. Jaouen, B. Hildebrand, M.-L. Mottas, M. Di Giovannantonio, P. Ruffieux, M. Rumo, C. W. Nicholson, E. Razzoli, C. Barreteau, A. Ubaldini, E. Giannini, F. Vanini, H. Beck, C. Monney, and P. Aebi, Phase separation in the vicinity of Fermi surface hot spots, Phys. Rev. B **100**, 075152 (2019).

[57] A. Abragam, *Principles of Nuclear Magnetism* (Oxford University Press, Oxford, 1961).

[58] E. Fukushima and S. B. W. Roeder, *Experimental Pulse NMR. a Nuts and Bolts Approach* (Addison-Wesley, Boca Raton, 1981).

[59] R. R. Ernst, G. Bodenhausen, and A. Wokaun, *Principles of Nuclear Magnetic Resonance in One and Two Dimensions* (Oxford University Press, Oxford, 1987).

[60] C. P. Slichter, *Principles of Magnetic Resonance*, 3rd ed. (Springer-Verlag, Berlin, 1990).

[61] M. H. Levitt, *Spin Dynamics. Basics of Nuclear Magnetic Resonance* (Wiley, Chichester, 2008).

[62] N. Bloembergen, E. M. Purcell, and R. V. Pound, Relaxation effects in nuclear magnetic resonance absorption, Phys. Rev. **73**, 679 (1948).

[63] R. Kubo and K. Tomita, A general theory of magnetic resonance absorption, J. Phys. Soc. Jpn. **9**, 888 (1954).

[64] C. Ritter, W. Müller-Warmuth, and R. Schöllhorn, Location of hydrogen in intercalation compounds of layered transition metal disulfides, a ^{1}H NMR study, Solid State Ion. **20**, 283 (1986).

[65] R. Dupree, W. W. Warren, and F. J. Di Salvo, ^{77}Se NMR study of the electronic instability in $TiSe_2$, Phys. Rev. B **16**, 1001 (1977).

[66] T. Tsuda, Y. Kitaoka, and H. Yasuoka, NMR studies of the CDW state in 1T-VSe_2, Physica B+C **105**, 414 (1981).

[67] T. Tsuda, H. Yasuoka, Y. Kitaoka, and F. J. Di Salvo, ^{51}V NMR study of the phase transition in 1T-VS_2, J. Magn. Magn. Mater. **31-34**, 1101 (1983).

[68] K. Mizuno, K. Magishi, Y. Shinonome, T. Saito, K. Koyama, N. Matsumoto, and S. Nagata, ^{125}Te NMR study of $IrTe_2$, Phys. B: Condens. Matter **312-313**, 818 (2002).

[69] M. Naito, H. Nishihara, and T. Butz, *Nuclear Spectroscopy on Charge Density Wave Systems* (Kluwer Academic, Dordrecht, 1992), pp. 35–112.

[70] A. V. Skripov, S. V. Rychkova, M. Y. Belyaev, and A. P. Stepanov, NMR study of hydrogen motion in hydrogen-stabilized C15-type compounds $ZrTi_2H_x$, Solid State Commun. **71**, 1119 (1989).

[71] A. V. Skripov, M. Y. Belyaev, and A. P. Stepanov, NMR study of hydrogen mobility in C14- and C15-type compounds $ZrCr_2H_x$, Solid State Commun. **78**, 909 (1991).

[72] A. V. Skripov, M. Y. Belyaev, S. V. Rychkova, and A. P. Stepanov, Nuclear magnetic resonance study of hydrogen diffusion in $HfV_2H_x(D_x)$ and $ZrV_2H_x(D_x)$: effects of phase transitions and isotope substitution, J. Phys.: Condens. Matter **3**, 6277 (1991).

[73] R. C. Bowman, D. R. Torgeson, and A. J. Maeland, Proton NMR studies of hydrogen diffusion behavior for $ZrBe_2H_{1.4}$, Z. Phys. Chem. **181**, 181 (1993).

[74] W. Küchler, P. Heitjans, A. Payer, and R. Schöllhorn, ^{7}Li NMR relaxation by diffusion in hexagonal and cubic Li_xTiS_2, Solid State Ion. **70-71**, 434 (1994).

[75] M. Wilkening, W. Küchler, and P. Heitjans, From Ultraslow to Fast Lithium Diffusion in the 2D Ion Conductor $Li_{0.7}TiS_2$ Probed Directly by Stimulated-Echo NMR and Nuclear Magnetic Relaxation, Phys. Rev. Lett. **97**, 065901 (2006).

[76] M. Wilkening and P. Heitjans, Li jump process in H-$Li_{0.7}TiS_2$ studied by two-time ^{7}Li spin-alignment echo NMR and comparison with results on two-dimensional diffusion from nuclear magnetic relaxation, Phys. Rev. B **77**, 024311 (2008).

[77] T. Wu, H. Mayaffre, S. Krämer, M. Horvatić, C. Berthier, W. N. Hardy, R. Liang, D. A. Bonn, and M.-H. Julien, Incipient charge order observed by NMR in the normal state of $YBa_2Cu_3O_y$, Nat. Commun. **6**, 6438 (2015).

[78] M. Spera, A. Scarfato, E. Giannini, and C. Renner, Energy-dependent spatial texturing of charge order in 1T-Cu_xTiSe_2, Phys. Rev. B **99**, 155133 (2019).

[79] F. Nad' and P. Monceau, Charge-density-wave glass state in quasi-one-dimensional conductors, Phys. Rev. B **51**, 2052 (1995).

[80] M.-H. Julien, F. Borsa, P. Carretta, M. Horvatić, C. Berthier, and C. T. Lin, Charge Segregation, Cluster Spin Glass, and Superconductivity in $La_{1.94}Sr_{0.06}CuO_4$, Phys. Rev. Lett. **83**, 604 (1999).

[81] M. Urai, K. Miyagawa, Y. Watanabe, E. I. Zhilyaeva, S. A. Torunova, R. N. Lyubovskaya, N. Drichko, and K. Kanoda, Anomalously field-susceptible spin clusters emerging in the electric-dipole liquid candidate κ-$(ET)_2Hg(SCN)_2Br$, Sci. Adv. **8**, eabn1680 (2022).

[82] F. Borsa, D. R. Torgeson, and H. R. Shanks, Charge-density wave amplitudes in 2H-$NbSe_2$ and 2H-$TaSe_2$ determined by ^{77}Se NMR, Phys. Rev. B **15**, 4576 (1977).

[83] A. V. Skripov, D. S. Sibirtsev, Y. G. Cherepanov, and B. A. Aleksashin, ^{77}Se NMR study of the charge density wave state in 2H-$NbSe_2$ and 1T-VSe_2, J. Phys.: Condens. Matter **7**, 4479 (1995).

[84] M. Barmatz, R. C. Farrow, and F. J. Di Salvo, Large elastic softening in the semimetal $TiSe_2$, *IEEE Ultrasonics Symposium Proceedings* (IEEE, Piscataway, NJ, 1977), p. 378.

[85] M. Barmatz, L. R. Testardi, and F. J. Di Salvo, Elasticity measurements in the layered dichalcogenides $TaSe_2$ and $NbSe_2$, Phys. Rev. B **12**, 4367 (1975).

[86] L. L. Lumata, K. Y. Choi, J. S. Brooks, A. P. Reyes, P. L. Kuhns, G. Wu, and X. H. Chen, ^{77}Se and ^{63}Cu NMR studies of the electronic correlations in Cu_xTiSe_2 ($x = 0.05$, 0.07), J. Phys.: Condens. Matter **22**, 295601 (2010).

[87] K. C. Woo, F. C. Brown, W. L. McMillan, R. J. Miller, M. J. Schaffman, and M. P. Sears, Superlattice formation in titanium diselenide, Phys. Rev. B **14**, 3242 (1976).

[88] D. R. P. Guy, R. H. Friend, D. C. Johnson, and M. J. Sienko, Magnetic susceptibility of hydrazine intercalated $TiSe_2$, J. Phys. C **15**, L1251 (1982).

[89] A. W. Overhauser, Observability of charge-density waves by neutron diffraction, Phys. Rev. B **3**, 3173 (1971).

[90] A. W. Overhauser, Phase excitations of charge density waves, Hyperfine Interact. **4**, 786 (1978).

[91] P. Bak, Commensurate phases, incommensurate phases and the devil's staircase, Rep. Prog. Phys. **45**, 587 (1982).

[92] R. Blinc, Magnetic resonance and relaxation in structurally incommensurate systems, Phys. Rep. **79**, 331 (1981).

[93] S. Zumer and R. Blinc, Nuclear spin-lattice relaxation in incommensurate systems, J. Phys. C **14**, 465 (1981).

[94] R. Blinc, D. C. Ailion, P. Prelovsek, and V. Rutar, Floating of the Modulation Wave and Phase Pinning in Incommensurate Rb_2ZnBr_4, Phys. Rev. Lett. **50**, 67 (1983).

[95] M. Kogoj, S. Zumer, and R. Blinc, Motion of the modulation wave and the NMR lineshape in incommensurate systems, J. Phys. C **17**, 2415 (1984).

[96] G. Papavassiliou, F. Milia, R. Blinc, and S. Zumer, Spin-lattice relaxation via floating of the incommensurate modulation wave in Rb_2ZnCl_4, Solid State Commun. **77**, 891 (1991).

[97] G. Papavassiliou, A. Anagnostopoulos, and F. Milia, Impurity pinning and thermally excited collective motions in incommensurately modulated structures, J. Phys.: Condens. Matter **5**, 9295 (1993).

[98] P. Matus, P. Bánki, and G. Kriza, ^{87}Rb NMR spin-lattice relaxation in the charge-density wave phase of $Rb_{0.3}MoO_3$, J. Phys. IV Proc. **9**, Pr10 (1999).

[99] B. Hildebrand, C. Didiot, A. M. Novello, G. Monney, A. Scarfato, A. Ubaldini, H. Berger, D. R. Bowler, C. Renner, and P. Aebi, Doping Nature of Native Defects in 1T$TiSe_2$, Phys. Rev. Lett. **112**, 197001 (2014).

[100] B. Hildebrand, T. Jaouen, M.-L. Mottas, G. Monney, C. Barreteau, E. Giannini, D. R. Bowler, and P. Aebi, Local Real-Space View of the Achiral 1T-$TiSe_2$ 2×2×2 charge density wave, Phys. Rev. Lett. **120**, 136404 (2018).

[101] L. Liu, C. Zhu, Z. Y. Liu, H. Deng, X. B. Zhou, Y. Li, Y. Sun, X. Huang, S. Li, X. Du, Z. Wang, T. Guan, H. Mao, Y. Sui, R. Wu, J.-X. Yin, J.-G. Cheng, and S. H. Pan, Thermal Dynamics of Charge Density Wave Pinning in $ZrTe_3$, Phys. Rev. Lett. **126**, 256401 (2021).

[102] X. Y. Feng, Z. Zhao, J. Luo, J. Yang, A. F. Fang, H. T. Yang, H. J. Gao, R. Zhou, and G.-Q. Zheng, Commensurate-to-incommensurate transition of charge-density-wave order and a possible quantum critical point in pressurized kagome metal CsV_3Sb_5, npj Quantum Mater. **8**, 23 (2023).

[103] X.-M. Wang and D.-L. Zhang, Effects of impurities and temperature on the thermal hysteresis of Ohmic resistance in Tl-doped blue bronze, Phys. Rev. B **54**, 1443 (1996).